A Characterization of the Immune Cells in Immunocompetent and Immunodeficient Mice with Orthotopic Brain Tumors.

Gardam B [1,2], Nam E [2,3], Kollis PM [1,2], Kilyen-Coles J [1,2], Lenin S [4], Gliddon BL [4], Tea MN [4], Pitson SM [1,4], Brown MP [1,2,5], Ebert LM [1,2,5], Gargett T [1,2,5].

[1] Adelaide Medical School The University of Adelaide, Adelaide, South Australia, Australia.
[2] Translational Oncology Laboratory, Centre for Cancer Biology, SA Pathology and University of South Australia, Adelaide, South Australia, Australia.
[3] Clinical and Health Sciences, University of South Australia, Adelaide, South Australia, Australia.
[4] Molecular Therapeutics Laboratory, Centre for Cancer Biology, SA Pathology and University of South Australia, Adelaide, South Australia, Australia.
[5] Cancer Clinical Trials Unit, Royal Adelaide Hospital, Adelaide, South Australia, Australia.

Abstract

Background: Glioblastoma, while considered rare, is characterized by poor survival and few treatment advances for over 20 years. New treatment options for brain cancers are, therefore, desperately needed. Active research that is being conducted in immunotherapy for glioblastoma and other primary brain cancers may be hampered by the lack of detailed studies that characterize the different immune compartments of orthotopic murine brain tumor models.

Methods: We used glioma neural stem cell lines derived from glioblastoma patients and murine glioma cell lines to produce intracranial xenograft and syngraft brain tumors in immunodeficient (NSG) or immunocompetent (C57BL/6) mice, respectively. High-parameter flow cytometry was used to characterize the immune cell compartment in each brain tumor model. We investigated the tissues of brain, spleen, lymph node, and bone marrow for the frequencies of monocytes, macrophages, B cells, T cells, dendritic cells, neutrophils, eosinophils, and where possible, their subsets.

Results: In a study first of non-tumor-bearing mice, we show dramatic differences between NSG and C57BL/6 mice in numbers not only of T and B cells but also of other immune cells. Then we show in mice bearing brain tumors significant differences in numbers of immune cells in brain, draining lymph nodes, spleen and bone marrow. Also, we investigated the effects on immune cell numbers of luciferase-expressing murine glioma cell lines compared to the parental lines. Finally, we show the effects of whole-body irradiation on immune cell numbers.

Conclusions: Our quantitative characterization of different immune compartments in orthotopic murine models of glioblastoma xenografts and syngrafts may allow for a better informed selection of tumor models that are appropriate for the pre-clinical investigation of immunotherapies for glioblastoma.

Introduction

Although brain and central nervous system cancers only represented 1.6% of newly diagnosed cancers in 2020, these cancers disproportionately represented 2.5% of the deaths for the same year [1]. A diagnosis of brain cancer comes with a poor prognosis and patient survival of 7-17 months [2]. There have been no life-prolonging advances in systemic therapies beyond the standard of care in the last 20 years [3] despite research activity that has been well-reviewed elsewhere [4]. Recently, immune-based therapies offer an exciting new approach for treating glioblastoma and include multiple clinical trials of immune checkpoint inhibitors, oncolytic viruses, autologous vaccines, and chimeric antigen receptor (CAR) T cells but with no apparent durable survival benefits [5,6]. One key challenge for developing new immunotherapies is finding animal models that enable the identification and measurement of effects of the immune intervention on immune targets and immune cells. Contributing to this challenge is a lack of detailed knowledge of the immune compartments in pre-clinical brain tumor models that may limit the ability of researchers to select the best model for investigating new immune-based treatments.

The different murine models of brain tumors, including (CT2A, GL261 and SB28) are well-characterized elsewhere [7]. Yet, although this publication provides a detailed description of the advantages and disadvantages of each model, there is no characterization of the immune compartments in these mice. Likewise, Khalsa et al. have performed a detailed characterization of the changes in the tumor-localized immune cells present within CT2A and GL261 syngraft models. However, changes in systemic immune composition were not characterized in primary and secondary lymphoid organs [8]. This is despite the fact that glioblastoma is now acknowledged to have profound effects on the systemic immune response [6,9-11]. To the best of our knowledge, there is currently no description of the baseline state of the immune system in brain tumor mouse models in the literature.

The immune-deficient NOD-SCID gamma null (NSG) mouse strain has been engineered to lack T, B and NK cells and together with a SIRPA polymorphism enables the successful engraftment of human cells. The NOD-SCID deficiencies allow the animals to accept a human tumor xenograft without immune rejection. In addition, several defects have been reported including that interleukin-2Rγ (IL-2Rγ) allelic mutations and the NOD genetic background of NSG mice impair lymph node organogenesis [12], the function of dendritic cells (DCs), which results in reduced interferon-gamma (IFN-γ) secretion, and the functional maturity of macrophages [13,14]. However, a limited range of markers has been applied to determine whether DC and macrophage dysfunction is generalized or limited to certain subsets, and the remaining immune compartments in NSG mice has been even less well described.

Moreover, there are conflicting reports on the use of reporter cell lines positive for firefly luciferase (luc) protein and the jellyfish green fluorescent protein (GFP) where it has been reported that luc and GFP expression can be immunogenic in some strains of mice [15]. In contrast, it has also been demonstrated that reporter gene expression in C57BL/6 mice is only minimally immunogenic [16]. Although most literature reports the effects of luc and GFP on tumor development and T cells, here, we will compare the immune cells in CT2A and GL261 tumor models with and without luc and GFP co-expression to determine the numerical changes in these cell types across different organs.

An improved understanding of the baseline immune state in mouse models of brain tumors and how well or not these recapitulate the human disease will contribute to the development of new immunotherapies. To address this question, we have investigated immune cell composition in three immunocompetent brain tumor models and two patient-derived xenograft glioblastoma models. Here, for the first time, we use high-parameter flow cytometry to systematically characterize the differences in immune cells in brain, spleen, draining lymph node, and bone marrow of C57BL/6 and NSG mice with and without brain tumors. Together, our findings provide important new knowledge of the baseline immune state in several mouse brain tumor models that are widely used in the field. This knowledge can be leveraged in future studies to select the most appropriate system for testing novel immunotherapies.

Results

We used a modified high-parameter flow cytometry panel, based on that described by Liu et al., to identify the immune cells in mice with and without orthotopic brain tumors [17]. In contrast to the individual detailed flow cytometry panels provided by Liu et al., we found that we could combine the individual panels into a single panel for analysis with careful consideration of the available fluorophores. We found this allowed for the identification of lymphocytes, granulocytes and monocytes (Fig 1A), dendritic cells (Fig 1B) and macrophages (Fig 1C) in the spleens, lymph nodes, bone marrow, and brains of the mice, as well as the microglia in the brains (Fig 1D). Microglia are defined by $CD45^{int}$ $CD11b^{+}$ $F4/80^{+}$ $Ly\text{-}6C^{-}$ in this panel, and are brain resident cells derived during embryonic development, distinct from infiltrating bone-marrow-derived myeloid lineages [18-20]. In addition, we have used a counting bead approach to enable reporting of both total numbers and proportions of immune cell types.

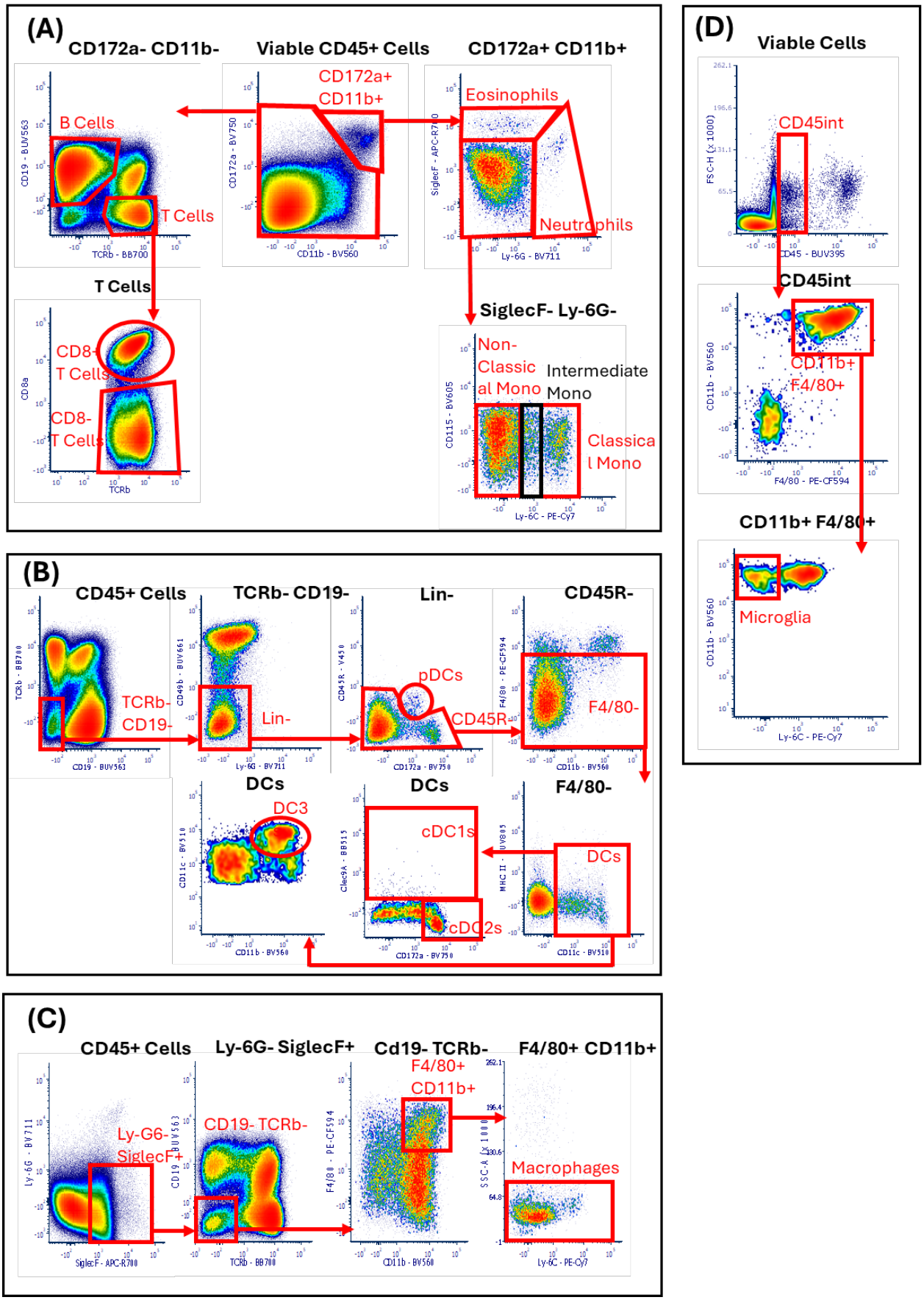

Figure 1. Indicative gating strategy for control C57BL/6 mouse to identify the murine immune cells. (A) Lymphocyte, monocyte and granulocyte gating, (B) Dendritic cell gating, (C) Macrophage gating, (D) Microglia gating.

Enumeration of immune cell types in non-tumor-bearing C57BL/6 and NSG mice

First, we compared the immune compartments in non-tumor-bearing (control) C57BL/6 and NSG mice. As expected, we identified no B or T cells in in all tissues of NSG mice (Fig 2A-D). In the brains, we observed a significant reduction in the number of eosinophils and a significant increase in the microglia in control NSG mice compared to control C57BL/6 mice (Fig 2A). In the spleens, we observed a significant increase in the macrophages in NSG mice compared to C57BL/6 mice, and a significant decrease in the monocytes, DCs and eosinophils in NSG compared to C57BL/6 mice (Fig 2B). We observed a significant decrease in the monocytes, DCs, neutrophils, and eosinophils in the lymph nodes of NSG mice compared to C57BL/6 mice (Fig 2C). Finally, in the bone marrow, we observed a significant decrease in macrophages, DCs, and eosinophils in the NSG compared to C57BL/6 mice (Fig 2D). The numerical defects observed in the immune cells of control NSG compared to C57BL/6 mice suggest that study of immune system-brain tumor interactions may be more limited in NSG mice, even for cells of the myeloid compartment, which have often been considered as relatively intact in NSG mice.

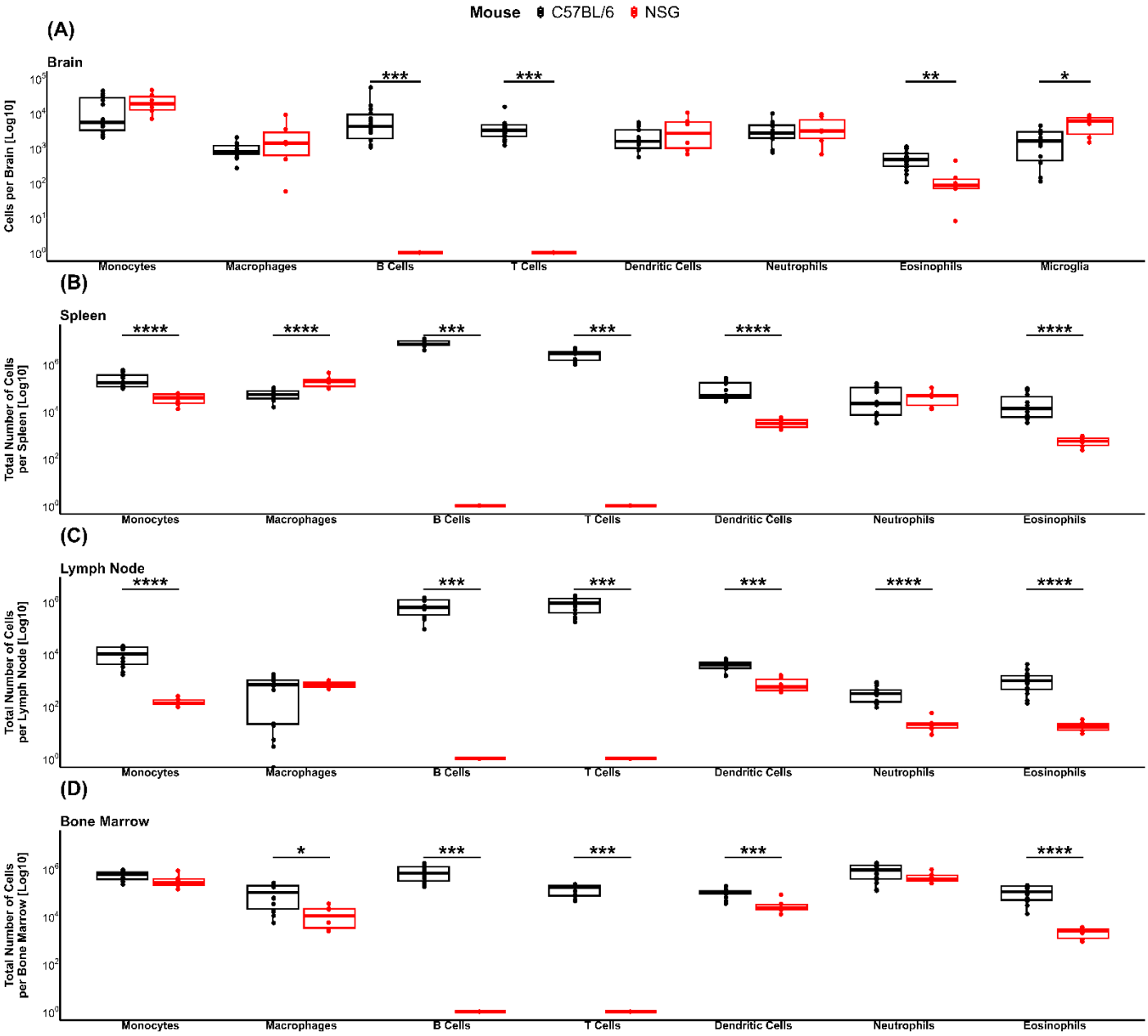

Figure 2. A comparison of immune cells in control C57BL/6 and NSG mice is shown as the total number per tissue. (A) Brain, (B) Spleen, (C) Lymph node, (D) Bone marrow. Data represent the median, second and third quartiles of n = 14 C57BL/6 mice and n = 6 NSG mice. P values *p<0.05, **P<0.01, ***p<0.001, ****p<0.0001.

Immune cell frequency distribution in C57BL/6 and NSG mice with or without orthotopic brain tumors

Next, we investigated immune cells in the brains, spleens, lymph nodes, and bone marrow of control mice compared to mice with orthotopic brain tumors. Tumor cells were surgically injected with a Stoelting motorized stereotactic frame into the brain's right hemisphere and allowed to grow for 3-4 weeks. All glioma cell lines had enforced expression of the disialoganglioside GD2, which is identical between mice and humans and which is expressed at low level in normal brain of both species [21]. In immunocompetent C57BL/6 mice, we assessed the effect of intracranial tumors of CT2A, CT2A-luc/GFP, GL261, GL261-luc/GFP, and SB28-luc/GFP glioma cell lines on the proportions of different leukocyte subsets (Fig 3A-D). As expected, the most dramatic differences in immune cell populations were observed in the brain. Mean, standard error of the mean (S.E.M) and p values are in Table S1. Specifically, we detected a significant increase in the proportion of monocytes in mice bearing CT2A, CT2A-luc/GFP and GL261 tumor-bearing mice compared to control mice, although unexpectedly, these cells were significantly reduced in the brains of mice bearing SB28-luc/GFP tumors. Notably, bone marrow-derived monocytes have been reported to support microglia in disease states and may be recruited before differentiation to supplement the brain resident microglia cells [18-20].

We also observed a significant decrease in B cells in the brains of all tumor-bearing mice compared to the control mice. We observed a significant increase in the percentage of dendritic cells in the brains of the CT2A-luc/GFP, GL261-luc/GFP, and SB28-luc/GFP tumor-bearing mice compared to control mice. Furthermore, we observed an increase in the percentage of T cells in the brains of CT2A-luc/GFP, and GL261-luc/GFP, and SB28-luc/GFP tumor-bearing mice compared to tumor-free mice (Fig 3A), with no apparent decrease in the spleen or increase in the bone marrow of the tumor-bearing mice despite previous reports [10] (Fig 3A, B, D). Of note, we did not see significant changes in most immune cell types in the spleens of the tumor-bearing compared to control mice, apart from an increase in the proportion T cells in the CT2A tumor-bearing model, a reduction in the macrophages and dendritic cells in the CT2A-luc/GFP model and dendritic cells in the SB28-luc/GFP tumor-bearing model (Fig 3B). There were also very few significant changes in the draining lymph nodes or bone marrow between tumor-bearing and control mice (Fig 3C-D).

In immunodeficient NSG mice, we assessed the effects of brain tumors generated from two different glioblastoma patient-derived glioma neural stem (GNS) cell lines, CCB-G4T-luc/GFP and CCB-G5C-luc/GFP [21,22] (Fig 3E-H). We observed an increase in the frequency of microglia in the brains of mice bearing either of the patient-derived tumors compared to control mice, with a corresponding decrease in monocyte frequency (Fig 3E). However, one of the most notable differences observed was the increase in "other immune cells" in the spleen, lymph node and bone marrow of NSG mice with or without a tumor compared to C57BL/6 mice; these are $CD45^+$ cells that do not have other lineage markers and that we consider to be immature or defective cells [23] (Fig 3F-H). Although there are other subtle changes in immune cell populations between mice bearing different tumors, these changes are considered in more detail below, where we assess the absolute numbers of these different immune cell subsets.

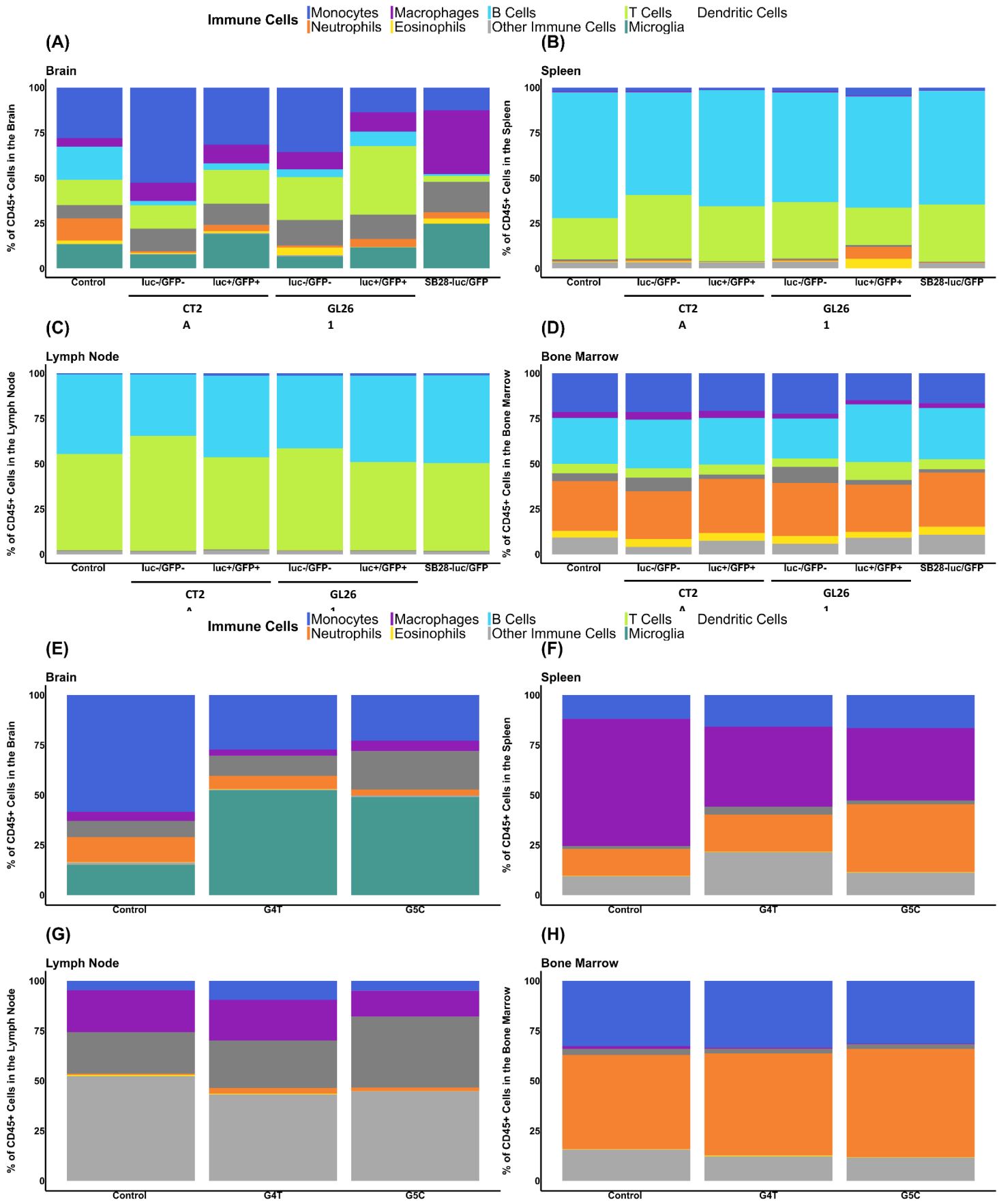

Figure 3. Immune cells as a percentage of the total CD45^{+} viable cells from (A) Brains of C57BL/6 mice, (B) Spleens of C57BL/6 mice, (C) Lymph nodes of C57BL/6 mice, (D) Bone marrow of C57BL/6 mice, (E) Brains of NSG mice, (F) Spleens of NSG mice, (G) Lymph nodes of NSG mice, (H) Bone marrow of NSG mice. Data represent the mean of n = 14 C57BL/6 mice, n = 11 CT2A tumor-bearing mice, n = 17 CT2A-luc/GFP tumor-bearing mice, n= 11GL261 tumor-bearing mice, n = 5 GL261-luc/GFP tumor-bearing mice, n = 5 SB28-luc/GFP tumor-bearing mice, n = 6 NSG mice, n = 6 G4T tumor-bearing mice, and n = 6 G5C tumor-bearing mice. P values *p<0.05, **P<0.01, ***p<0.001, ****p<0.0001.

Enumeration of immune cell types in C57BL/6 with orthotopic brain tumors with or without luciferase and GFP

As the immunogenic properties of luciferase-expressing (luc) cells have been reported as minimal in C57BL/6 mice [16] and evident in other strains [15], we first quantified differences in immune cell composition between the luc-expressing and non-expressing GL261 and CT2A cell lines implanted as orthotopic brain tumor models (Fig S1). To summarize these findings, we observed changes in immune cell number between tumors with and without reporter genes. However, it did not appear that the reporter molecules were immunogenic in terms of the number of tumor-infiltraing cells in the brain (Fig S1A,E). Nonetheless, the changes observed in the spleens of the CT2A tumor-bearing models could indicate an increased immune response in the CT2A-luc/GFP tumor-bearing model (Fig S1B), an effect not observed in the GL261 tumor-bearing models (Fig S1F).

Absolute numbers of immune cell types in C57BL/6 mice with or without orthotopic brain tumors

Although the analysis above revealed several changes in immune cell type frequencies between control and tumor-bearing mice, it is also important to consider potential changes in absolute numbers. Following our analysis of the differences between the tumors expressing luciferase/GFP and those not expressing luciferase, we have focused this analysis on luciferase-expressing models because we believed that being able to monitor the tumor growth was more important than differences in immune cell composition that may result from the potential immunogenicity of reporter molecules.

Figure 4A shows the number of each immune cell type within brains of immunocompetent tumor-bearing and control mice. First, we observed a significant increase in the number of monocytes in brains of CT2A-luc/GFP tumor-bearing mice and SB28-luc/GFP tumor-bearing mice compared to control C57BL/6 mice, and a significant increase in macrophages in all brains of mice bearing the syngeneic tumors compared to the control C57BL/6 mice. Second, we observed a significant increase in T cells in brains of the CT2A-luc/GFP and GL261-luc/GFP tumor-bearing mice compared to control C57BL/6 mice. Interestingly, SB28-luc/GFP tumor-bearing mice were not observed to have the same increase in T cells. Third, DCs in the brains of SB28-luc/GFP and CT2A-luc/GFP tumor-bearing mice were also significantly increased compared to control C57BL/6 mice, and eosinophils were significantly increased in the CT2A-luc/GFP tumor-bearing mice compared to control C57BL/6 mice. Finally, we observed a significant increase in microglia in the CT2A-luc/GFP and SB28-luc/GFP tumor-bearing mice compared to control C57BL/6 mice (Fig 4A).

When considering the systemic immune changes, we observed a significant decrease in splenic DCs of CT2A-luc/GFP and SB28-luc/GFP tumor-bearing mice compared to control C57BL/6 mice and a significant decrease in splenic neutrophils and eosinophils in CT2A-luc/GFP tumor-bearing mice compared to control C57BL/6 mice (Fig 4B). Remarkably, we observed no significant changes in any of the immune cell subsets in draining lymph nodes in the immunocompetent models (Fig 4C). Finally, we observed a significant increase in total monocytes in bone marrow of SB28-luc/GFP tumor-bearing mice compared to the GL261-luc/GFP tumor-bearing mice (Fig 4D).

In summary, these analyses of immunocompetent brain tumor models reveal a significant increase in brain infiltrating immune cells of CT2A-luc/GFP tumor-bearing bearing mice, and to a lesser extent in SB28-luc/GFP tumor-bearing mice compared to the control mice while spleens of tumor-bearing mice show a trend toward fewer immune cells than in control mice.

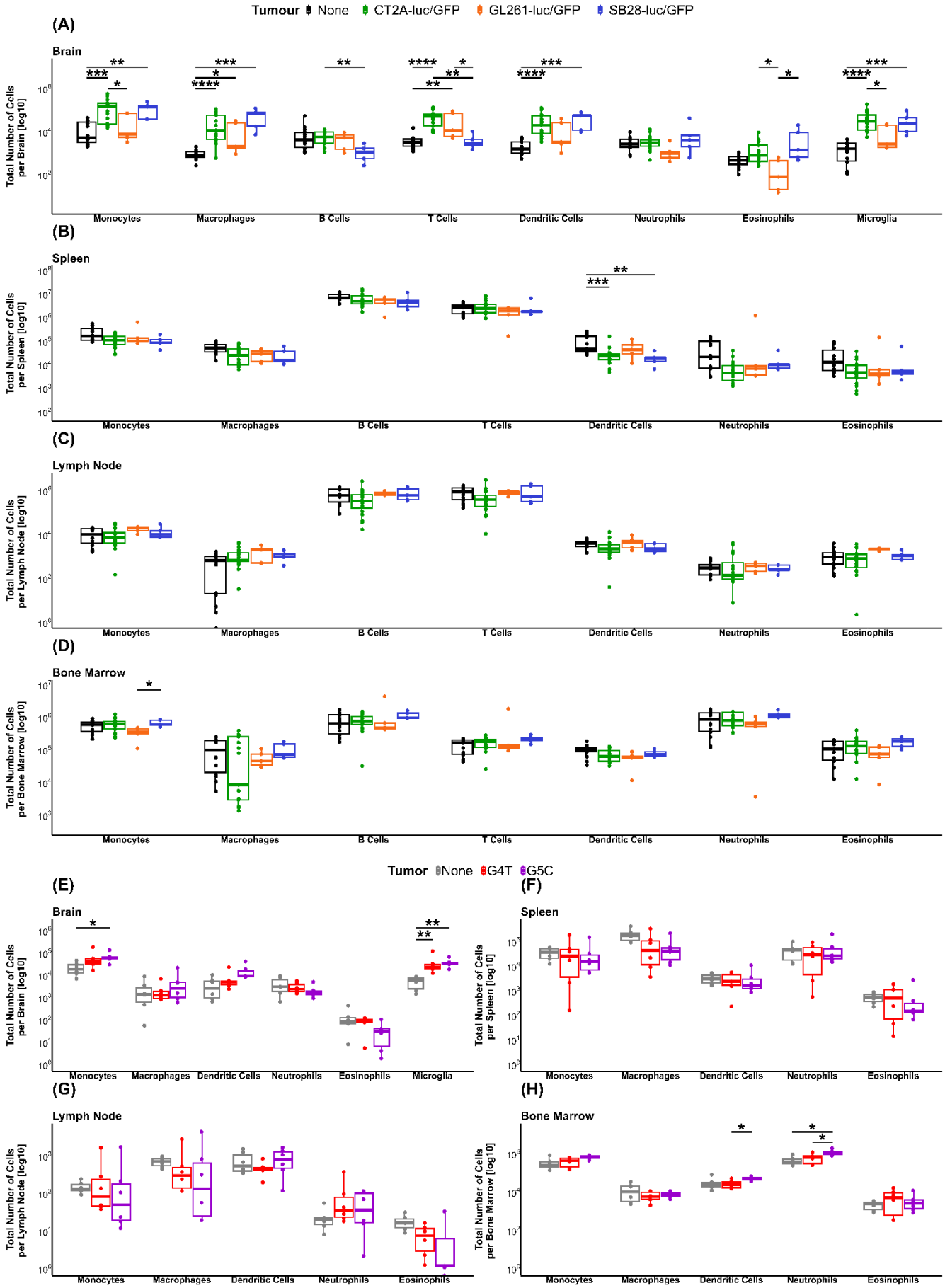

Figure 4. Absolute numbers of immune cell populations in control mice and mice with the indicated orthotopic brain tumors. Graphs analyze immunocompetent C57BL/6 mice (A—D), or immunodeficient NSG mice (E-G). (A, E) Brains, (B, F) Spleens, (C, G) Lymph Nodes, (D, H) Bone marrow B cells and T cells are not shown for the NSG models as they are deficient in these cell types. Data represent the median, second and third quartiles of n = 14 C57BL/6 mice, n = 17 CT2A-luc/GFP tumor-bearing mice, n = 5 GL261-luc/GFP tumor-

bearing mice, n = 5 SB28-luc/GFP tumor-bearing mice, n = 6 NSG mice, n = 6 G4T tumor-bearing mice, and n = 6 G5C tumor-bearing mice. P values *p<0.05, **P<0.01, ***p<0.001, ****p<0.0001.

Absolute numbers of immune cell types in NSG mice with or without orthotopic brain tumors

Next, we investigated the immunodeficient models. In the brain, we observed a significant increase in total monocytes in G5C-luc/GFP tumor-bearing mice compared to control NSG mice and a significant increase in microglia in all tumor-bearing mice compared to control NSG mice (Fig 4E), which is consistent with our findings in immunocompetent models. In contrast, we observed no significant changes in spleen or draining lymph node of immunodeficient models (Fig 4F-G). Finally, we observed a significant increase of neutrophils in bone marrow of G5C-luc/GFP tumor-bearing mice compared to control NSG mice and no differences in any other cell type (Fig 4H). Overall, a brain tumor in NSG mice had little effect on immune cell populations of the mice.

Enumeration of T cell, monocyte and DC subsets in brain tumor models

Given the diversity that exists within immune cell types, we next investigated the subsets of immune cells in greater detail. We performed sub-analyses of monocytes to enumerate classical phagocytic monocytes, non-classical inflammatory antigen cross-presenting monocytes, and transitional intermediate monocytes [24]. We also subdivided T cells into $CD8^+$ and $CD8^-$ subsets, and differentiated between anti-tumor cross-presenting classical dendritic cells type 1 (cDC1s), pro-tumor classical dendritic cells type 2 (cDC2s), and inflammatory dendritic cells type 3 (DC3s).

In considering the brains of immunocompetent mice (Fig 5A), we observed a significant increase in classical and non-classical monocytes, but not intermediate monocytes, in CT2A-luc/GFP and SB28-luc/GFP tumor-bearing mice compared to control C57BL/6 mice. When analysing $CD8^+$ and $CD8^-$ T cells separately, we observed the same trends as for bulk T cells, with both subsets being increased in the CT2A-luc/GFP and GL261-luc/GFP models, but not in the SB28-luc/GFP model, compared to control mice. In DC subsets, we observed a significant increase in the cDC2s and DC3s in CT2A-luc/GFP and SB28-luc/GFP mice compared to control C57BL6 mice, whereas cDC1 numbers were unchanged.

Many changes in these immune cell subsets were also observed elswhere in the immune system. In the spleen (Fig 5B), we observed a significant increase in non-classical monocytes in all tumor-bearing mice compared to control C57BL/6 mice. There were very few changes to T cell subsets, with the only difference being a significant decrease in $CD8^+$ T cells in GL261-luc/GFP tumor-bearing mice compared to control C57BL/6 mice. For DCs, we observed a significant decrease in splenic cDC1s and cDC2s of SB28-lucGFP mice, while there was only a significant decrease in cDC1s in CT2A-luc/GFP tumor-bearing mice compared to control C57BL/6 mice. Within draining lymph nodes, we observed a significant increase in the intermediate monocytes in GL261-luc/GFP and SB28-luc/GFP tumor-bearing mice compared to control C57BL/6 mice, and a significant decrease in $CD8^+$ T cells in CT2A-luc/GFP tumor bearing mice compared to control C57BL/6 mice (Fig 5C). Finally, we examined the bone marrow (Fig 5D), where we observed a significant increase in classical monocytes in CT2A-luc/GFP and SB28-luc/GFP tumor-bearing mice and a significant decrease in intermediate monocytes in GL261-luc/GFP mice compared to control C57BL/6 mice.

We then investigated changes to leukocyte subsets in the immunodeficient models. In the brain, we observed a significant increase in non-classical monocytes and DC3s in both tumor-bearing models compared to the control NSG mice (Fig 5E). In contrast, no significant changes were observed in spleen or draining lymph node (Fig 5F-G), whereas we observed a significant increase of non-classical monocytes in bone marrow of G5C-luc/GFP mice compared to the control NSG mice (Fig 5H).

Together, these detailed analyses reveal that most changes in immune cell subsets occur in brain and spleen of tumor-bearing mice, with minimal changes in the composition of immune cell subsets in draining lymph node and bone marrow. Meanwhile, the NSG mice showed very few changes in immune cell subsets in the tumor-bearing mice compared to control mice.

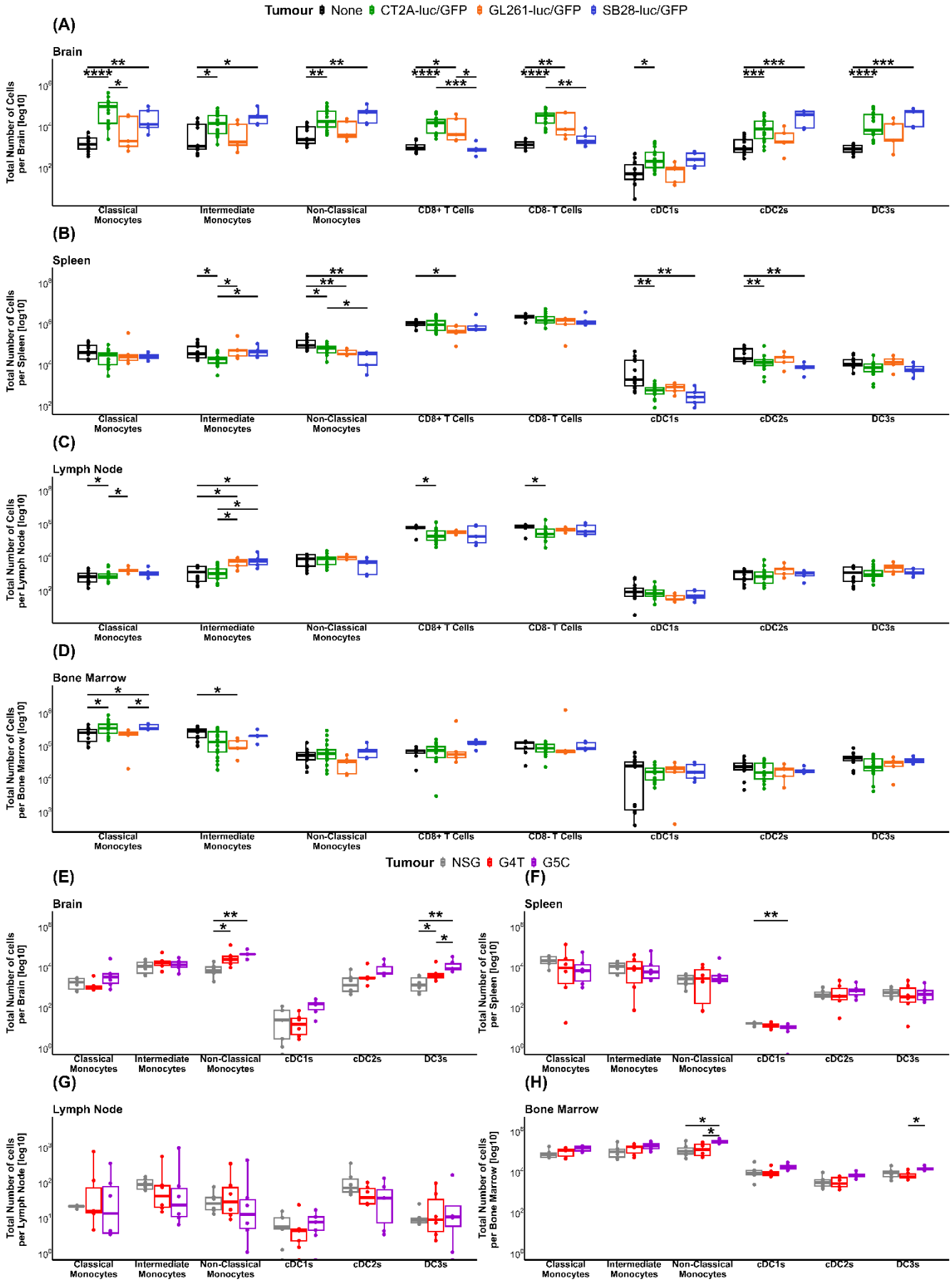

Figure 5. Absolute numbers of monocyte, T cell and DC subsets, in control mice and mice with the indicated orthotopic brain tumors. Graphs analyze immunocompetent C57BL/6 mice (A—D), or immunodeficient NSG mice (E-G). (A, E) Brains, (B, F) Spleens, (C, G) Lymph Nodes, (D, H) Bone marrow B cells and T cells are not shown for the NSG models as they are deficient in these cell types. Data represent the median, second and third quartiles of n = 14 C57BL/6 mice, n = 17 CT2A-luc/GFP tumor-bearing mice, n = 5 GL261-luc/GFP

tumor-bearing mice, n = 5 SB28-luc/GFP tumor-bearing mice, n = 6 NSG mice, n = 6 G4T tumor-bearing mice, and n = 6 G5C tumor-bearing mice. P values *p<0.05, **P<0.01, ***p<0.001, ****p<0.0001

Effect of whole body irradiation on immune cell types

We then considered the effects of whole-body sub-lethal x-ray irradiation on the CT2A-luc/GFP tumor-bearing mice. Sub-lethal irradiation is frequently used to achieve lymphodepletion in mice before other immunotherapies such as CAR-T cells, to promote effective engraftment of adoptively transferred cells [25,26]. Irradiation is also reported, at least initially, reduce immunosuppression by depleting pro-tumor immune cells such as tumor associated macrophages as well as increase tumor immunogenicity by both upregulating expression of damage-associated molecular pattern molecules and inducing tumor cell death that results in release of and increased presentation of tumor antigen [27].

To evaluate the effects of whole-body (sub-lethal) irradiation (WBI) on control mice, we irradiated C57BL/6 mice with a range of X-ray doses from 0.5 Gy to 5 Gy, then analyzed immune cells in spleen, peripheral blood, and bone marrow. For initial analyses, we enumerated bulk $CD45^+$ immune cells (Fig 6A) and observed a significant decrease in the spleen at all WBI doses compared to control C57BL/6 mice, with the most marked decrease seen at the 5 Gy dose. Although we observed no significant changes in peripheral blood numbers of $CD45^+$ cells at any WBI dose compared to control C57BL/6 mice, there was a trend toward reduced numbers of circulating $CD45^+$ immune cells at higher WBI doses. We also observed a significant reduction in $CD45^+$ immune cells in bone marrow of mice treated with 5 Gy WBI compared to all other mice.

Next, we treated CT2A-luc/GFP tumor-bearing mice with 5 Gy WBI 7 days after tumor cell implantation. At the euthanasia endpoint (approximately four weeks after tumor cell implantation), we compared the immune cells in these irradiated mice to mice bearing CT2A-luc/GFP tumors that did not receive WBI. In brain, we observed a significant reduction in macrophages, B cells, DCs, and neutrophils when tumor-bearing mice received 5 Gy WBI than when they did not. (Fig 6B). In spleen (Fig 6C), we observed a significant reduction in B cells and T cells but a significant increase in monocytes, macrophages, neutrophils and eosinophils in WBI-treated mice compared to untreated CT2A-luc/GFP tumor-bearing mice. In the draining lymph nodes (Fig 7D), we again observed a significant reduction in B cells and T cells following irradiation. Finally, in the bone marrow, we observed a significant increase in monocytes and neutrophils in the WBI-treated mice compared to the untreated CT2A-luc/GFP tumor-bearing mice, while all of the other immune cells were unaffected by WBI (Fig 7E). Taken together, this would suggest that most immune cells have returned to normal levels by euthanasia endpoint post-WBI. Two exceptions to this trend include the tumor-bearing brains, where many immune cell populations were still altered following WBI, and in B cells and T cells, which seem to take longer to repopulate spleen and draining lymph node than other immune cells.

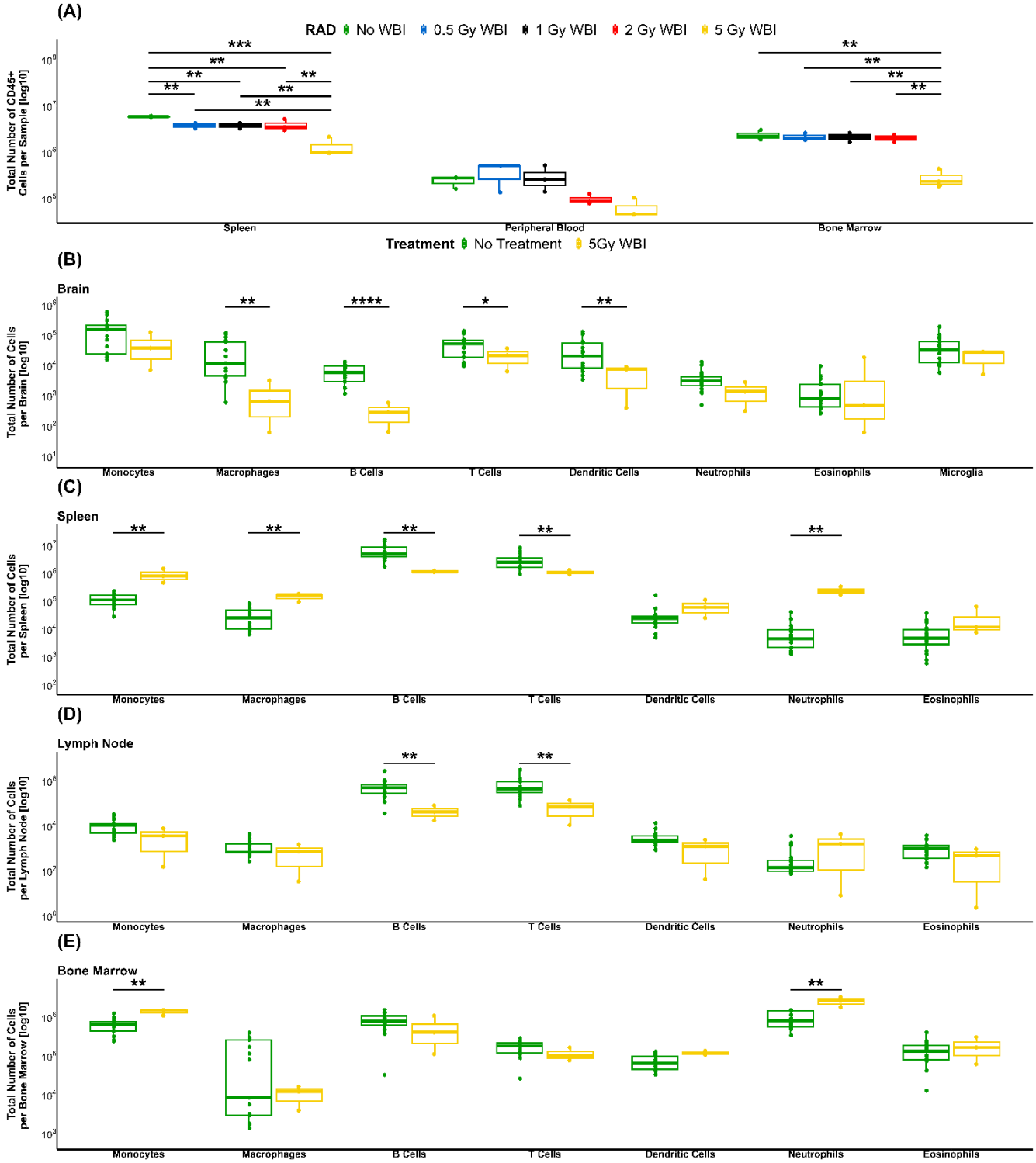

Figure 6. Immune cells in C57BL/6 mice with and without whole body x-ray irradiation. (A) dose comparison in tumor-free mice, analyzing the total number of $CD45^+$ leukocytes in the spleen, peripheral blood and bone marrow. (B) immune cells in the brains of CT2A-luc/GFP tumor-bearing mice with and without WBI, (C) immune cells in the spleens of CT2A-luc/GFP tumor-bearing mice with and without WBI, (D) immune cells in the draining lymph nodes of CT2A-luc/GFP tumor-bearing mice with and without WBI, (E) immune cells in the bone marrow of CT2A-luc/GFP tumor-bearing mice with and without WBI. Data represent the median, second and third quartiles of n = 3 per group for male total $CD45^+$ mice, n = 17 CT2A-luc/GFP tumor-bearing mice, and n = 3 5Gy WBI CT2A-luc/GFP tumor-bearing mice. P values *p<0.05, **P<0.01, ***p<0.001, ****p<0.0001.

Discussion

Although the immunotherapy revolution has transformed the treatment paradigm for many cancers, it does not play a part in the standard treatment of glioblastoma patients and thus remains an active area of research [6,28,29]. Immunotherapy approaches such as immune-checkpoint inhibitors may be useful in < 3% of patients whereas although CAR-T cell therapy may have broader application, early-phase clinical trial data are limited [30-32]. Further research is required to find ways to allow immune therapies to combat features of the glioblastoma tumor microenvironment limiting immune activity including antigen heterogeneity and a phalanx of immunosuppressive molecules and cell types particularly those of myeloid origin [33,34]. Moreover, in glioblastoma, the immune suppression extends system-wide and includes DC dysfunction, lymphopenia, T-cell sequestration and elevated circulating myeloid-derived suppressor cells (MDSCs) [10,35-40]. To develop effective immune-based treatments, it is, therefore, essential that we have appropriate pre-clinical models that recapitulate these features of glioblastoma. During our own efforts, however, we found little information about system-wide immune compartments in commonly used orthotopic murine brain tumor models. Consequently, we have undertaken detailed studies to examine system-wide immune compartments in control NSG and C57BL/6 mice and in the same strains of mice hosting intracranial brain tumors.

One aspect of our studies focussed on better defining the immune system of control NSG mice. Previous reports have described immature macrophages and dysfunctional DCs [13,14]. We now build on these previous findings by revealing significant changes in the absolute numbers of several immune cell types in multiple organs, when comparing control NSG mice to control immune competent C57BL/6 mice. In particular, we identified that monocytes and DCs were significantly reduced in the spleens and lymph nodes of NSG mice, and eosinophils were significantly reduced in all tissues analyzed, compared to C5BL/6 mice. Interestingly, these systemic reductions in monocytes and DCs did not extend to the brain, where NSG mice showed a significant increase in microglia numbers and no changes to monocyte or DC numbers in the NSG mice compared to C57BL/6 mice.

With the inoculation of brain tumors in the C57BL/6 mice, we observed a significant increase in the classical and non-classical monocytes, macrophages, $CD8^+$ and $CD8^-$ T cells, cDC2s, DC3s, and microglia in the brains of the CT2A-luc/GFP tumor-bearing mice compared to control C57BL/6 mice. Further, we observed the same significant increases with the exception of the T cells in the brains of the SB28-luc/GFP tumor-bearing mice compared to control C57BL/6 mice. In contrast, in the brains of the GL261-luc/GFP tumor-bearing mice, we only observed a significant increase in the macrophages, $CD8^+$ and $CD8^-$ T cells compared to control C57BL/6 mice. In the immunodeficient NSG models, we observed a significant increase in populations of non-classical monocytes and microglia in both of our tumor-bearing models compared to the control NSG mouse. These data suggest that the expression of luc and GFP had little to no effect on the immune system in these mice.

Given the intriguing findings of glioblastoma-mediated global immune suppression by others [10,35-40], we wished also to investigate lymphoid organs such as the spleen and bone marrow of tumor-bearing mice. In immunocompetent C57BL/6 mice, we found that the presence of a brain tumor induced few changes in the bone marrow, and we did not observe the previously reported [10] sequestration of T cells in this site. We also observed no changes in lymph nodes. In the spleens of tumor-bearing mice, DCs, neutrophils and eosinophils were reduced, but no changes were observed in other populations. Our study, therefore supports the concept that brain tumors induce some level of systemic immune suppression in mice, but this is not as profound or widespread as previously reported. Furthermore, this effect was not observed in NSG models, where the presence of a brain tumor did not lead to systemic reductions in any immune cell types beyond the immune defects already present within this strain. Limitations of our studies include investigating only syngraft models, which are acknowledged to be less biologically similar to human glioblastoma than genetically engineered models [7], and not examining the functional satus of the enumerated immune cells, which remains an area for future investigation.

In addition, we investigated the effect of reporter gene expression on immune cell composition. Although GFP has been reported by others to have minimal immunogenicity in C57BL/6 mice [15,16], to our knowledge, few

data exist beyond GFP effects on T cells and tumor cells. We found only a few changes in immune cell populations in the GL261-luc/GFP tumor-bearing mice compared to the GL261 tumor-bearing mice. However, the CT2A-luc/GFP tumor-bearing mice had significant changes in all splenic immune cell populations compared to the CT2A tumor-bearing mice. Only a significant change in a single immune cell population was found in other tissues of these mice. Consequently, the technical benefits of these models such longitudinal bioluminescence imaging of growth of luc-expressing tumors and tracking of GFP-expressing tumor cells in downstream analyses should be weighed against possible artefactual effects of luc and GFP expression on immune cell composition as we observed in these tumor models.

Finally, we addressed the effects of WBI on the immune system. WBI is used routinely in syngraft models to achieve CAR-T engraftment [25,26], yet the immune effects are rarely considered. We found that at the euthanasia endpoint, there was a significant reduction in B cells and T cells in brain, spleen, and draining lymph node and a non-significant reduction in B and T cells in bone marrow of irradiated mice. We also observed a significant increase in monocytes, macrophages, neutrophils, and eosinophils in spleen of WBI mice. Importantly, we have shown that use of WBI in these models has effects beyond transient lymphodepletion and, in fact, in our study, there appears to be broad remodelling of the immune system following WBI, which will have consequences for any immune-targeted treatment.

This study highlights the importance of a broad assessment of immune cell numbers when deciding which pre-clinical model is appropriate for testing immune-based therapies. NSG mice are routinely used for xenograft models of CAR-T therapy because they enable human tumor and human T cells to be assessed. However, as we have shown, there are extensive differences in system-wide immune cell composition beyond the absence of B and T cells, and including a broad reduction in DCs, monocytes and eosinophils. Therefore, it will be difficult to adequately assess the endogenous immune effects of approaches that rely on systemic immune engagement, such as cytokine-enabled CAR-T [21,41] or other combination therapy approaches [42-44]. However, we did observe that system-wide reductions in numbers of monocytes and DCs did not apply in the brain. These data suggest that, despite numerical and functional impairments at steady state, myeloid cell populations in NSG mice are responsive to the emergency demands imposed by the pathology of a brain tumor. Consequently, these data suggest that NSG brain tumor models may be suitable for studies of immunotherapies targeting myeloid cells, and for investigating interactions between CAR-T cell therapies and the local brain tumor immune microenvironment, which is typically dominated by macrophages and microglia. Nevertheless, further studies are needed to better define the function of these brain-resident myeloid cells in NSG mice.

In conclusion, this study presents a global overview of immune cell numbers in commonly used pre-clinical models of glioblastoma. In considering immunocompetent syngraft models, all three models had evidence of immunogenic tumors with extensive immune cell infiltration of the brain tumor, which is not reported for human glioblastoma and without the evidence of extensive systemic immune suppression described by others [10]. The SB28 model did appear most closely to represent human glioblastoma because the levels of T cells in the brain are the lowest and there is some level of T cell sequestration. Although the immunodeficient NSG models showed an increase in monocytes and microglia in the brains, other immune cells remained virtually unchanged in the presence of a brain tumor. Together, these findings will enable researchers in the field of glioblastoma immunotherapy to better interpret their results and we hope will support further development of immunotherapy for this devastating disease.

Materials and Methods

Patient-Derived Glioblastoma Cell Lines.

The patient-derived GNS cell lines were generated as previously described [45]. Briefly, an aliquot of dissociated glioblastoma cells was resuspended in 3 mL StemPro NSC medium (Thermo Fisher) and transferred to a T-25 tissue culture flask coated for 30 min at 37°C with Matrigel (Corning Incorporated, Corning, NY, USA) diluted 1/100 in PBS. The following day, the flask was rinsed twice with warm DMEM to remove debris and dead cells, and fresh StemPro NSC was added. All GNS cell cultures were passaged when they reached 70–

95% confluence by detaching cells using StemPro Accutase (Thermo Fisher) and seeding fresh Matrigel-coated flasks at a 1:3 to 1:5 split ratio. Cultures were grown in a humidified incubator at 37°C with 5% CO_2.

Orthotopic Brain Tumor Models

Animal experiments were conducted under a protocol approved by the University of South Australia Animal Ethics Committee (#32-22 & #U08-23). A Stoelting motorized stereotactic alignment and injection unit was used to deliver 2 µL of tumor cells to the brain over a period of 4 minutes, 3 mm deep into the right hemisphere. Syngraft models were generated by the implantation of GD2-SB28-luc/GFP cells (5×10^3 cells), GD2-CT2A cells (5×10^4 cells), GD2-CT2A-luc/GFP cells (5×10^4 cells), GD2-GL261 cells (1×10^5 cells), and GD2-GL261-luc/GFP cells (1×10^5 cells) into 6–8 weeks old female C57BL/6 mice (Australian BioResources, Moss Vale). Patient-derived cell lines G5C-luc/GFP (2×10^5 cells), and G4T-luc/GFP (5×10^5 cells) were injected into 6-8 weeks old female NSG mice (Ozgene, Perth). Mice received daily clinical checks and weekly bioluminescence imaging (BLI) for mice with luciferase expression to monitor tumor growth. BLI was performed using an IVIS Lumina S5 after intraperitoneal injection of 100 µL of 30 mg/mL luciferin in saline. Defined euthanasia endpoints included loss of >15% body weight from starting weight, a body condition score of <2 (under-conditioned)[46], and neurological signs including head-tilt, loss of balance and circling movement.

Murine Whole-body Irradiation

Whole-body irradiation was conducted in X-Rad225 (Precision X-ray irradiation, Madison, CT). Each dose was calculated using an internal probe to deliver a total effective dose of 0.5 Gy, 1 Gy, 2 Gy, or 5 Gy.

Murine Tissue Samples.

Spleens, bone marrow, from the left rear leg, draining lymph nodes and brains were harvested from euthanized mice and mechanically dissociated utilizing 40 µm strainers in Roswell Park Memorial Institute (RPMI) 1640 Medium (ThermoFisher Scientific, Cat# 11875093) + 1% Foetal Bovine Serum (FBS) (CellSera, Cat# AU-FBS/PG). Samples were centrifuged at 400g for 5 min and resuspended in FBS + 10% dimethyl sulfoxide (DMSO) (Sigma-Aldrich, Cat# D8418) and cryopreserved for later analysis.

Flow Cytometry Staining and Analysis

Cryopreserved dissociated tissue samples were rapidly thawed in a 37°C water bath and transferred to tubes containing 9 mL of warm RPMI. After 10 min at RT, cells were centrifuged and resuspended in FACS buffer (PBS, 0.01%, sodium azide, 0.5% BSA), and Fc receptors were blocked with Mouse BD Fc Block (BD Biosciences, Cat# 553141) for 10 min at room temperature (RT). Cells were then incubated for 30 min at RT with cocktails containing Brilliant Staining Buffer Plus (BD Biosciences, Cat# 564220), True-Stain Monocyte Blocker (BioLegend, Cat# 421103) and combinations of the antibodies in Table S2. After washing twice in PBS, cells were incubated with a fixable viability stain for 30 min at RT, washed in FACS buffer, resuspended in FACS buffer, and stored at 4° C until acquisition on the same day. Samples were transferred to TruCount tubes (BD Biosciences, Cat# 340334) to enable absolute cell numbers to be determined.

All samples were acquired on a BD FACSymphony A5 using FACS Diva Software (BD Biosciences). Analysis was performed using FCS Express v7 Flow Research Edition (De Novo Software, Pasadena, CA, USA).

Statistical Analysis

Data was graphed and analyzed using Rstudio Version 2023.06.1. Statistical analysis was conducted in Rstudio utilizing the Kruskal-Wallis test and the Pairwise Wilcoxon test with Benjamini & Hochberg multiple comparison post-tests. P values <0.05 were considered statistically significant.

Funding

Funding for this study was provided by Cancer Australia and the Kids Cancer Project (PdCCRS grant 2020344).

Acknowledgments

BG acknowledges the support received from the NeuroSurgical Research Foundation. The authors also acknowledge the support of the South Australian Neurological Tumor Bank (SANTB) for the provision of patient tumor samples for the generation of the patient-derived glioma neural stem cell lines. The authors also acknowledge the assistance of the staff of the Core Animal Facility at the University of South Australia with the experiments. We acknowledge Steven Roberts (BD Biosciences) for technical advice in designing multicolour flow panels for use on the BD FACS Symphony. The authors also acknowledge the support of the Adelaide Health and BioMedical Precinct Cytometry Facility SAHMRI, the Facility is generously supported by the Detmold Group, McMahon Family, Australian Cancer Research Foundation, Cancer Council and Australian Government through the Zero Childhood Cancer Program.

Data Availability

Data will be made available upon reasonable request.

Conflict of interest

The authors report no conflict of interest.

Author Information

Contributions

Conceptualization (BG, TG, MPB, LME), Data Collection and Analysis (BG, EN, PMK, JK) Animal Surgery (BLG, MNT, SL) First Draft (BG), Critical Review and Editing (BG, TG, BLG, MNT, SMP, MPB, LME, TG)

Supplementary Information

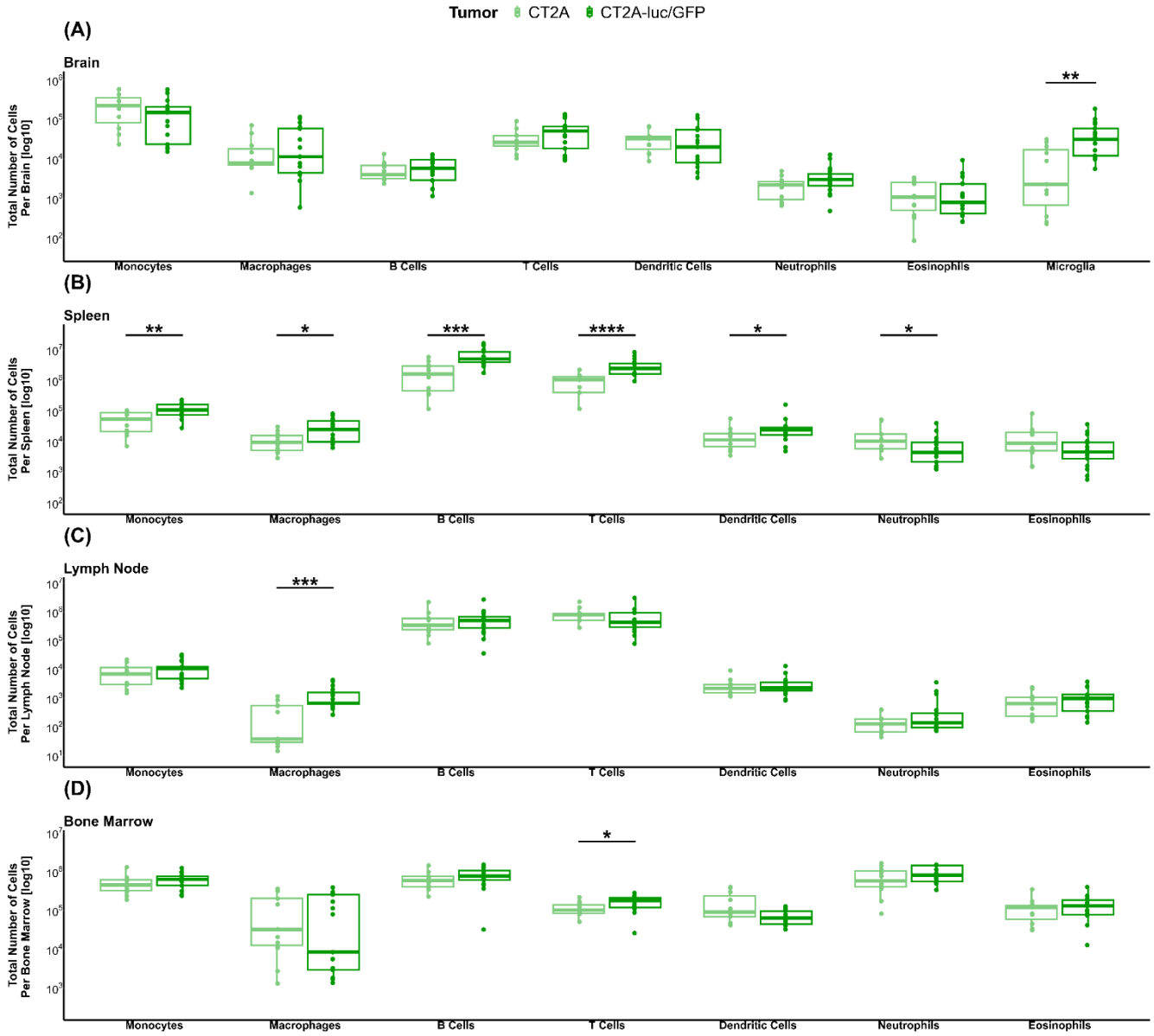
Tumor
CT2A
CT2A-luc/GFP
(A)
Brain
Total Number of Cells Per Brain [log10]
Monocytes
Macrophages
B Cells
T Cells
Dendritic Cells
Neutrophils
Eosinophils
Microglia
**
(B)
Spleen
Total Number of Cells Per Spleen [log10]
**
*
***
****
*
*
Monocytes
Macrophages
B Cells
T Cells
Dendritic Cells
Neutrophils
Eosinophils
(C)
Lymph Node
Total Number of Cells Per Lymph Node [log10]
***
Monocytes
Macrophages
B Cells
T Cells
Dendritic Cells
Neutrophils
Eosinophils
(D)
Bone Marrow
Total Number of Cells Per Bone Marrow [log10]
*
Monocytes
Macrophages
B Cells
T Cells
Dendritic Cells
Neutrophils
Eosinophils

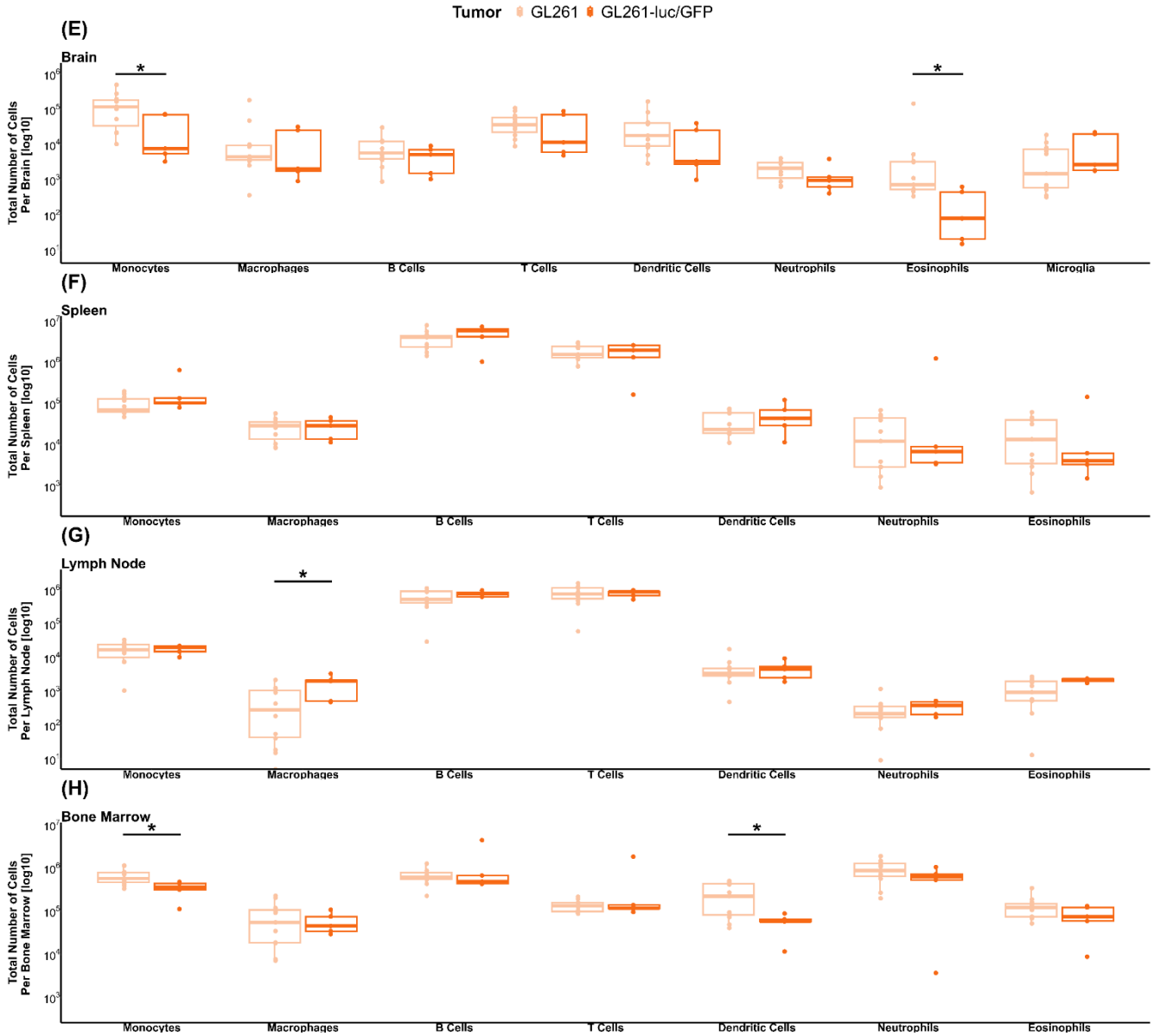

Figure S1. A comparison of CT2A (A-D) and GL261 (E-G) cells in orthotopic tumors expressing or not expressing a luciferase/GFP reporter gene cassette in the Brains (A, E), Spleens (B, F) Draining lymph nodes (C, G), and bone marrow (D, H), of C57BL/6 mice. Data represent the median, second and third quartiles of n = 11 CT2A tumor-bearing mice, n = 17 CT2A-luc/GFP tumor-bearing mice, n = 11 GL261 tumor-bearing mice, n = 5 GL261-luc/GFP tumor-bearing mice P values *p<0.05, **P<0.01, ***p<0.001, ****p<0.0001.

Table S1. Percentage of $CD45^+$ immune cells in mice with orthotopic tumors in C57BL/6 and NSG mice. Data showes mean S.M.E and P values. P values *p<0.05, **P<0.01, ***p<0.001, ****p<0.0001.

P Values * ** *** ****

Brain

Cells	Healthy n =14		CT2A n=11			CT2A-luc/GFP n=17			GL261 n=11			GL261-luc/GFP n=5			SB28-luc/GFP		
	Mean	S.E.M	Mean	S.E.M	P Value	Mean	S.E.M	P Value	Mean	S.E.M	P Value	Mean	S.E.M	P Value	Mean	S.E.M	P Value
Monocytes	27.910	3.391	52.599	2.945	0.00013	31.521	3.616	0.00555	35.651	4.006	0.01166	13.707	3.085	1.00000	12.503	2.932	0.00086
Macrophages	4.768	0.919	10.033	3.170	0.69940	10.343	2.021	0.07670	9.548	3.867	0.69940	10.567	1.995	0.06450	35.360	5.372	0.00260
B Cells	18.261	1.907	2.443	0.608	3.4E-06	3.617	0.852	7.9e-07	4.283	1.178	6.7e-05	8.071	2.002	0.01030	0.898	0.220	0.00064
T Cells	13.989	1.874	12.904	2.310	0.88970	18.638	0.937	0.03910	23.621	4.391	0.15010	37.821	1.782	0.00130	3.341	0.898	0.00210
Dendritic Cells	7.404	0.780	12.523	2.255	0.22340	11.899	1.209	0.03470	14.193	3.088	0.09510	13.401	2.242	0.03570	16.844	2.554	0.00130
Neutrophils	12.257	2.284	0.948	0.333	6.7e-06	3.286	1.246	0.00021	1.212	0.237	6.7e-06	4.438	2.087	0.15748	3.463	1.431	0.16318
Eosinophils	1.908	0.281	0.474	0.131	0.00130	1.172	0.601	0.00210	4.180	3.465	0.02850	0.204	0.040	0.00130	2.866	1.109	0.68680
Microglia	13.498	3.663	7.837	3.054	0.21170	19.039	3.298	0.37190	6.599	4.300	0.22970	11.582	2.424	0.96440	24.669	8.436	0.37190

Spleen

Cells	Healthy n =14		CT2A n=11			CT2A-luc/GFP n=17			GL261 n=11			GL261-luc/GFP n=5			SB28-luc/GFP		
	Mean	S.E.M	Mean	S.E.M	P Value	Mean	S.E.M	P Value	Mean	S.E.M	P Value	Mean	S.E.M	P Value	Mean	S.E.M	P Value
Monocytes	2.103	0.321	2.028	0.192	0.91300	1.225	0.108	0.24200	2.099	0.508	0.86300	4.424	3.176	0.91300	1.326	0.157	0.84900
Macrophages	0.477	0.058	0.525	0.126	0.83900	0.283	0.035	0.04500	0.521	0.115	0.83900	0.348	0.036	0.70700	0.363	0.105	0.70700
B Cells	69.558	1.598	56.845	3.106	0.02700	64.130	1.604	0.13000	60.782	2.888	0.11400	61.602	8.588	0.57700	62.862	2.462	0.16400
T Cells	22.823	2.025	35.116	2.869	0.05100	30.352	1.777	0.07900	31.125	2.709	0.07900	20.653	4.153	0.89300	31.821	2.545	0.07900
Dendritic Cells	0.840	0.168	0.714	0.140	0.95300	0.301	0.057	0.01300	0.804	0.211	1.00000	0.982	0.566	1.00000	0.244	0.023	0.02500
Neutrophils	0.451	0.118	0.806	0.178	0.31750	0.104	0.028	0.26850	0.540	0.188	0.91160	6.616	6.543	0.91160	0.261	0.139	0.91160
Eosinophils	0.247	0.064	0.606	0.168	0.08090	0.107	0.030	0.10880	0.493	0.146	0.60440	0.805	0.575	0.60440	0.206	0.145	0.81600

Lymph Node

Cells	Healthy n =14		CT2A n=11			CT2A-luc/GFP n=17			GL261 n=11			GL261-luc/GFP n=5			SB28-luc/GFP		
	Mean	S.E.M	Mean	S.E.M	P Value	Mean	S.E.M	P Value	Mean	S.E.M	P Value	Mean	S.E.M	P Value	Mean	S.E.M	P Value
Monocytes	0.647	0.061	0.535	0.069	0.57270	1.060	0.123	0.03210	1.313	0.218	0.03210	1.094	0.101	0.03210	0.923	0.175	0.34860
Macrophages	0.029	0.009	0.019	0.007	0.86180	0.133	0.021	0.00110	0.046	0.019	0.90220	0.105	0.031	0.07380	0.088	0.031	0.07960
B Cells	43.906	2.264	33.907	3.046	0.09000	45.241	2.458	1.00000	40.133	2.299	0.48600	47.768	2.581	0.57700	48.584	3.171	0.48900
T Cells	53.218	2.155	63.733	3.116	0.05000	50.945	2.375	0.89000	56.186	2.220	0.55000	48.858	2.442	0.45000	48.577	3.385	0.45000
Dendritic Cells	0.280	0.027	0.237	0.054	0.30000	0.306	0.037	0.92000	0.324	0.045	0.86000	0.293	0.074	0.87000	0.192	0.043	0.30000
Neutrophils	0.035	0.012	0.016	0.005	0.76000	0.037	0.010	1.00000	0.020	0.004	0.93000	0.022	0.004	1.00000	0.026	0.010	1.00000
Eosinophils	0.079	0.018	0.060	0.013	0.74300	0.090	0.009	0.30000	0.093	0.024	0.74300	0.136	0.013	0.14500	0.088	0.025	0.74300

Bone Marrow

Cells	Healthy n =14		CT2A n=11			CT2A-luc/GFP n=17			GL261 n=11			GL261-luc/GFP n=5			SB28-luc/GFP		
	Mean	S.E.M	Mean	S.E.M	P Value	Mean	S.E.M	P Value	Mean	S.E.M	P Value	Mean	S.E.M	P Value	Mean	S.E.M	P Value
Monocytes	21.309	1.668	21.313	1.727	0.96000	20.812	1.391	0.98000	22.405	1.679	0.90000	14.839	3.362	0.83000	16.553	0.370	0.39000
Macrophages	3.327	0.506	4.227	1.271	1.00000	3.931	1.042	1.00000	2.560	0.709	1.00000	2.345	0.562	1.00000	2.584	0.640	1.00000
B Cells	25.472	1.118	26.994	2.370	0.86700	25.776	1.690	0.86100	21.970	1.010	0.22100	31.821	8.949	0.86100	28.331	1.140	0.53300
T Cells	5.038	0.295	5.124	0.454	0.98000	5.406	0.310	0.92000	4.800	0.383	0.92000	9.889	4.532	0.90000	5.415	0.308	0.92000
Dendritic Cells	4.286	0.588	7.406	1.705	0.43000	2.444	0.243	0.03600	8.790	2.050	0.43000	2.531	0.654	0.43000	1.950	0.117	0.03600
Neutrophils	27.626	2.062	26.450	2.868	1.00000	29.950	1.243	1.00000	29.336	2.622	1.00000	26.085	6.620	1.00000	29.934	1.438	1.00000
Eosinophils	3.684	0.236	4.439	0.419	1.00000	4.197	0.340	1.00000	4.248	0.423	1.00000	3.427	0.864	1.00000	4.385	0.675	1.00000

Brain

Cells	NSG n=6		G4T n=6			G5C n=6		
	Mean	S.E.M	Mean	S.E.M	P Value	Mean	S.E.M	P Value
Monocytes	58.329	4.711	27.289	2.907	0.00650	22.825	2.262	0.00650
Macrophages	4.546	1.295	3.010	0.357	0.94000	5.156	1.750	0.94000
B Cells	0.000		0.000			0.000		
T Cells	0.000		0.000			0.000		
Dendritic Cells	8.124	1.127	10.088	0.813	0.31000	19.238	3.048	0.03900
Neutrophils	12.389	4.695	6.659	1.869	0.39400	3.018	0.864	0.04500
Eosinophils	0.270	0.049	0.160	0.050	0.24000	0.045	0.017	0.01300
Microglia	15.128	3.952	52.376	2.478	0.00320	49.008	4.143	0.00320

Spleen

Cells	NSG n=6		G4T n=6			G5C n=6		
	Mean	S.E.M	Mean	S.E.M	P Value	Mean	S.E.M	P Value
Monocytes	11.943	1.659	15.778	3.486	0.36000	16.559	1.791	0.28000
Macrophages	63.606	4.042	40.061	3.543	0.00650	36.094	3.693	0.00650
B Cells	0.000		0.000			0.000		
T Cells	0.000		0.000			0.000		
Dendritic Cells	1.374	0.427	3.900	2.371	0.59000	1.959	0.154	0.40000
Neutrophils	13.449	2.598	18.562	5.513	0.69900	33.956	4.358	0.01300
Eosinophils	0.197	0.041	0.302	0.053	0.46000	0.233	0.041	0.59000

Lymph Node

Cells	NSG n=6		G4T n=6			G5C n=6		
	Mean	S.E.M	Mean	S.E.M	P Value	Mean	S.E.M	P Value
Monocytes	4.684	1.209	9.496	3.659	0.82000	4.921	1.991	0.82000
Macrophages	20.925	3.279	20.380	5.256	1.00000	12.994	5.538	0.46000
B Cells	0.000		0.000			0.000		
T Cells	0.000		0.000			0.000		
Dendritic Cells	20.754	3.905	23.663	3.901	0.70000	35.418	10.405	0.70000
Neutrophils	0.659	0.166	2.840	0.667	0.01300	1.789	0.564	0.18000
Eosinophils	0.597	0.186	0.418	0.150	0.39400	0.071	0.042	0.02300

Bone Marrow

Cells	NSG n=6		G4T n=6			G5C n=6		
	Mean	S.E.M	Mean	S.E.M	P Value	Mean	S.E.M	P Value
Monocytes	32.637	1.772	33.327	1.410	0.82000	31.292	1.892	0.82000
Macrophages	1.354	0.503	0.592	0.122	0.13200	0.353	0.029	0.02600
B Cells	0.000		0.000			0.000		
T Cells	0.000		0.000			0.000		
Dendritic Cells	3.013	0.284	2.434	0.223	0.27000	2.387	0.144	0.27000
Neutrophils	47.204	2.482	51.003	1.243	0.20000	54.163	1.761	0.12000
Eosinophils	0.248	0.062	0.489	0.173	0.48000	0.154	0.049	0.40000

Table S2. Antibodies that were used for staining murine tissue samples for the identification of immune cells.

Antibody	Conjugate	Clone	Supplier	Catalogue #
Viability	FVS 780		BD Biosciences	565388
CD45	BUV395	30-F11	BD Biosciences	564279
FcεR1α	BUV496	MAR-1	BD Biosciences	751763
CD172a	BV750	P84	BD Biosciences	747007
CD11b	BV650	M1/70	BD Biosciences	563402
CD19	BUV563	1D3	BD Biosciences	749028
TCR b	BB700	H57-597	BD Biosciences	745846
CD49b	BUV661	HMα2	BD Biosciences	741523
Ly-6G	BV711	1A8	BD Biosciences	563979
CD45R	V450	MAR-1	BD Biosciences	751763
F4/80	PE-CF594	T45-2342	BD Biosciences	565613
I-A/I-E (MHC II)	BUV805	2G9	BD Biosciences	748707
CD11c	BV510	N418	BD Biosciences	744178
Clec9A (CD370)	BB515	10B4	BD Biosciences	565320
Ly-6C	PE-Cy7	AL-21	BD Biosciences	560593
Siglec-F	APC-R700	E50-2440	BD Biosciences	565183
CD115	BV605	T38-320	BD Biosciences	743640
PD-L1 (CD274)	BUV615	MIH5	BD Biosciences	752339
CCR7 (CD197)	AF647	4B12	BD Biosciences	560766
CD86	BUV737	PO3	BD Biosciences	741757
CD8a	PE	5H10-1	BD Biosciences	567630

References.

1 Sung, H. *et al.* Global Cancer Statistics 2020: GLOBOCAN Estimates of Incidence and Mortality Worldwide for 36 Cancers in 185 Countries. *CA: A Cancer Journal for Clinicians* **71**, 209-249, doi:https://doi.org/10.3322/caac.21660 (2021).

2 Nguyen, H.-M., Guz-montgomery, K., Lowe, D. B. & Saha, D. Pathogenetic features and current management of glioblastoma. *Cancers* **13**, 1-42, doi:10.3390/cancers13040856 (2021).

3 Stupp, R. *et al.* Radiotherapy plus Concomitant and Adjuvant Temozolomide for Glioblastoma. *New England Journal of Medicine* **352**, 987-996, doi:10.1056/NEJMoa043330 (2005).

4 Baddam, S. R., Kalagara, S., Kuna, K. & Enaganti, S. Recent advancements and theranostics strategies in glioblastoma therapy. *Biomedical Materials* **18**, 052007, doi:10.1088/1748-605X/acf0ab (2023).

5 Maccari, M. *et al.* Present and Future of Immunotherapy in Patients With Glioblastoma: Limitations and Opportunities. *The Oncologist* **29**, 289-302, doi:10.1093/oncolo/oyad321 (2023).

6 Gardam, B., Gargett, T., Brown, M. P. & Ebert, L. M. Targeting the dendritic cell-T cell axis to develop effective immunotherapies for glioblastoma. *Frontiers in Immunology* **14**, doi:10.3389/fimmu.2023.1261257 (2023).

7 Haddad, A. F. *et al.* Mouse models of glioblastoma for the evaluation of novel therapeutic strategies. *Neuro-Oncology Advances* **3**, doi:10.1093/noajnl/vdab100 (2021).

8 Khalsa, J. K. *et al.* Immune phenotyping of diverse syngeneic murine brain tumors identifies immunologically distinct types. *Nature Communications* **11**, 3912, doi:10.1038/s41467-020-17704-5 (2020).

9 Himes, B. T. *et al.* Immunosuppression in Glioblastoma: Current Understanding and Therapeutic Implications. *Front Oncol* **11**, 770561, doi:10.3389/fonc.2021.770561 (2021).

10 Chongsathidkiet, P. *et al.* Sequestration of T cells in bone marrow in the setting of glioblastoma and other intracranial tumors. *Nature Medicine* **24**, 1459-1468, doi:10.1038/s41591-018-0135-2 (2018).

11 Ayasoufi, K. *et al.* Brain cancer induces systemic immunosuppression through release of non-steroid soluble mediators. *Brain* **143**, 3629-3652, doi:10.1093/brain/awaa343 (2020).

12 Takahashi, T. *et al.* Enhanced Antibody Responses in a Novel NOG Transgenic Mouse with Restored Lymph Node Organogenesis. *Frontiers in Immunology* **Volume 8 - 2017**, doi:10.3389/fimmu.2017.02017 (2018).

13 Shultz, L. D. *et al.* Human Lymphoid and Myeloid Cell Development in NOD/LtSz-scid IL2Rγnull Mice Engrafted with Mobilized Human Hemopoietic Stem Cells 12. *The Journal of Immunology* **174**, 6477-6489, doi:10.4049/jimmunol.174.10.6477 (2005).

14 Ito, M. *et al.* NOD/SCID/γcnull mouse: an excellent recipient mouse model for engraftment of human cells. *Blood* **100**, 3175-3182, doi:https://doi.org/10.1182/blood-2001-12-0207 (2002).

15 Grzelak, C. A. *et al.* Elimination of fluorescent protein immunogenicity permits modeling of metastasis in immune-competent settings. *Cancer Cell* **40**, 1-2, doi:https://doi.org/10.1016/j.ccell.2021.11.004 (2022).

16 Skelton, D., Satake, N. & Kohn, D. B. The enhanced green fluorescent protein (eGFP) is minimally immunogenic in C57BL/6 mice. *Gene Therapy* **8**, 1813-1814, doi:10.1038/sj.gt.3301586 (2001).

17 Liu, Z., Gu, Y., Shin, A., Zhang, S. & Ginhoux, F. Analysis of Myeloid Cells in Mouse Tissues with Flow Cytometry. *STAR Protocols* **1**, 100029, doi:https://doi.org/10.1016/j.xpro.2020.100029 (2020).

18 Choi, B.-R., Johnson, K. R., Maric, D. & McGavern, D. B. Monocyte-derived IL-6 programs microglia to rebuild damaged brain vasculature. *Nature Immunology* **24**, 1110-1123, doi:10.1038/s41590-023-01521-1 (2023).

19 Spiteri, A. G., Wishart, C. L. & King, N. J. C. Immovable Object Meets Unstoppable Force? Dialogue Between Resident and Peripheral Myeloid Cells in the Inflamed Brain. *Frontiers in Immunology* **11**, doi:10.3389/fimmu.2020.600822 (2020).

20 Spiteri, A. G. *et al.* High-parameter cytometry unmasks microglial cell spatio-temporal response kinetics in severe neuroinflammatory disease. *Journal of Neuroinflammation* **18**, 166, doi:10.1186/s12974-021-02214-y (2021).

21 Gargett, T. *et al.* GD2-targeting CAR-T cells enhanced by transgenic IL-15 expression are an effective and clinically feasible therapy for glioblastoma. *J Immunother Cancer* **10**, e005187, doi:10.1136/jitc-2022-005187 (2022).

22 Pollard, S. M. *et al.* Glioma stem cell lines expanded in adherent culture have tumor-specific phenotypes and are suitable for chemical and genetic screens. *Cell Stem Cell* **4**, 568-580, doi:10.1016/j.stem.2009.03.014 (2009).

23 Dudek, A. M., Martin, S., Garg, A. D. & Agostinis, P. Immature, Semi-Mature, and Fully Mature Dendritic Cells: Toward a DC-Cancer Cells Interface That Augments Anticancer Immunity. *Front Immunol* **4**, 438, doi:10.3389/fimmu.2013.00438 (2013).

24 Mukherjee, R. *et al.* Non-Classical monocytes display inflammatory features: Validation in Sepsis and Systemic Lupus Erythematous. *Scientific Reports* **5**, 13886, doi:10.1038/srep13886 (2015).

25 Tennant, M. D., New, C., Ferreira, L. M. R. & O'Neil, R. T. Efficient T cell adoptive transfer in lymphoreplete hosts mediated by transient activation of Stat5 signaling. *Molecular Therapy* **31**, 2591-2599, doi:10.1016/j.ymthe.2023.07.015 (2023).
26 Johnson, C. B. *et al.* Enhanced Lymphodepletion Is Insufficient to Replace Exogenous IL2 or IL15 Therapy in Augmenting the Efficacy of Adoptively Transferred Effector CD8+ T Cells. *Cancer Research* **78**, 3067-3074, doi:10.1158/0008-5472.Can-17-2153 (2018).
27 Donlon, N. E., Power, R., Hayes, C., Reynolds, J. V. & Lysaght, J. Radiotherapy, immunotherapy, and the tumour microenvironment: Turning an immunosuppressive milieu into a therapeutic opportunity. *Cancer Letters* **502**, 84-96, doi:https://doi.org/10.1016/j.canlet.2020.12.045 (2021).
28 Liu, Y., Zhou, F., Ali, H., Lathia, J. D. & Chen, P. Immunotherapy for glioblastoma: current state, challenges, and future perspectives. *Cellular & Molecular Immunology* **21**, 1354-1375, doi:10.1038/s41423-024-01226-x (2024).
29 Salvato, I. & Marchini, A. Immunotherapeutic Strategies for the Treatment of Glioblastoma: Current Challenges and Future Perspectives. *Cancers* **16**, 1276 (2024).
30 Omuro, A. *et al.* Nivolumab with or without ipilimumab in patients with recurrent glioblastoma: results from exploratory phase I cohorts of CheckMate 143. *Neuro-oncology* **20**, 674-686 (2018).
31 Omuro, A. *et al.* Nivolumab plus radiotherapy with or without temozolomide in newly diagnosed glioblastoma: Results from exploratory phase I cohorts of CheckMate 143. *Neuro-oncology advances* **4**, vdac025-vdac025, doi:10.1093/noajnl/vdac025 (2022).
32 Agosti, E. *et al.* Glioblastoma immunotherapy: A systematic review of the present strategies and prospects for advancements. *International Journal of Molecular Sciences* **24**, 15037 (2023).
33 Yeo, E. C. F., Brown, M. P., Gargett, T. & Ebert, L. M. The Role of Cytokines and Chemokines in Shaping the Immune Microenvironment of Glioblastoma: Implications for Immunotherapy. *Cells (Basel, Switzerland)* **10**, 607, doi:10.3390/cells10030607 (2021).
34 Sharma, P., Aaroe, A., Liang, J. & Puduvalli, V. K. Tumor microenvironment in glioblastoma: Current and emerging concepts. *Neurooncol Adv* **5**, vdad009, doi:10.1093/noajnl/vdad009 (2023).
35 Gieryng, A., Pszczolkowska, D., Walentynowicz, K. A., Rajan, W. D. & Kaminska, B. Immune microenvironment of gliomas. *Laboratory Investigation* **97**, 498-518, doi:10.1038/labinvest.2017.19 (2017).
36 Gousias, K., von Ruecker, A., Voulgari, P. & Simon, M. Phenotypical analysis, relation to malignancy and prognostic relevance of ICOS + T regulatory and dendritic cells in patients with gliomas. *Journal of neuroimmunology* **264**, 84-90, doi:10.1016/j.jneuroim.2013.09.001 (2013).
37 Löhr, M. *et al.* High-grade glioma associated immunosuppression does not prevent immune responses induced by therapeutic vaccines in combination with T reg depletion. *Cancer immunology, immunotherapy* (2018).
38 Sheu, T.-T. & Chiang, B.-L. Lymphopenia, Lymphopenia-Induced Proliferation, and Autoimmunity. *International journal of molecular sciences* **22**, 4152, doi:10.3390/ijms22084152 (2021).
39 Grossman, S. A. *et al.* Immunosuppression in Patients with High-Grade Gliomas Treated with Radiation and Temozolomide. *Clinical Cancer Research* **17**, 5473-5480, doi:10.1158/1078-0432.Ccr-11-0774 (2011).
40 Ghosh, S. *et al.* Radiation-induced circulating myeloid-derived suppressor cells induce systemic lymphopenia after chemoradiotherapy in patients with glioblastoma. *Science translational medicine* **15**, eabn6758, doi:10.1126/scitranslmed.abn6758 (2023).
41 Tang, L., Pan, S., Wei, X., Xu, X. & Wei, Q. Arming CAR-T cells with cytokines and more: Innovations in the fourth-generation CAR-T development. *Molecular Therapy* **31**, 3146-3162, doi:10.1016/j.ymthe.2023.09.021 (2023).
42 Ageenko, A., Vasileva, N., Richter, V. & Kuligina, E. Combination of Oncolytic Virotherapy with Different Antitumor Approaches against Glioblastoma. *International Journal of Molecular Sciences* **25**, 2042 (2024).
43 Segura-Collar, B. *et al.* Advanced immunotherapies for glioblastoma: tumor neoantigen vaccines in combination with immunomodulators. *Acta Neuropathologica Communications* **11**, 79, doi:10.1186/s40478-023-01569-y (2023).
44 Houweling, M. *et al.* Screening of predicted synergistic multi-target therapies in glioblastoma identifies new treatment strategies. *Neuro-Oncology Advances* **5**, doi:10.1093/noajnl/vdad073 (2023).
45 Ebert, L. M. *et al.* Endothelial, pericyte and tumor cell expression in glioblastoma identifies fibroblast activation protein (FAP) as an excellent target for immunotherapy. *Clinical & Translational Immunology* **9**, e1191, doi:https://doi.org/10.1002/cti2.1191 (2020).
46 Ullman-Culleré, M. H. & Foltz, C. J. Body condition scoring: a rapid and accurate method for assessing health status in mice. *Lab Anim Sci* **49**, 319-323 (1999).